The interaction of a surface cold front with a prefontal thermodynamically well-mixed boundary layer

Michael J. Reeder, General Sciences Corporation, Laurel, and Laboratory for Atmospheres, NASA/Goddard Space Flight Center, Greenbelt, Maryland, USA.

(Manuscript received July 1986; revised November 1986)

The idealised two-dimensional numerical model of Reeder and Smith (1987) is extended to investigate the dynamics of a surface cold front, initially at sea, as it propagates onshore and encounters a thermodynamically well-mixed boundary layer resulting from diurnal heating. The effect of heating on the transverse frontal circulation is shown to be locally profound. An intense prefrontal updraft develops in the late afternoon, accompanied by rapid unbalanced *in situ* frontogenesis and an increase in the speed of frontal propagation. When heating is excluded, the magnitude of the low-level cross-front wind component is everywhere less than the speed of propagation of the front, whereas when diabatic heating is added the low-level cross-front wind component immediately behind the front becomes greater than the frontal speed. It is shown that these results cannot be interpreted simply as a superposition of the frontal circulation and a sea-breeze, nor can they be attributed to symmetric instability. Comparison of the model with observations of Australian summertime cold fronts shows substantial agreement. Implications for the circumstances under which fronts develop gravity-current-like features are discussed.

Introduction

The modern description of atmospheric fronts rests upon seminal contributions by Sawyer (1956) and Eliassen (1959, 1962), who investigated the instantaneous cross-front (transverse) circulation associated with a two-dimensional front. Subsequently, Stone (1966) and Williams and Plotkin (1968) examined the time-dependent frontal formation process in the context of quasi-geostrophic theory wherein, *inter alia*, the momentum is approximated by the geostrophic momentum, and ageostrophic advections are neglected. The analytic theory of frontogenesis culminated in the work of Hoskins and Bretherton (1972), who successfully employed what are now known as the semi-geostrophic equations to incorporate the crucial effect of ageostrophic advection of the geostrophic wind and potential temperature.

Each of the foregoing theories assumes, *inter alia*, that the time-scale on which the flow accelerates is in some sense large compared to the inertial time-scale, and that the system, at all times, maintains cross-front thermal wind balance. Indeed, the accompanying transverse circulation is precisely that required to preserve cross-front thermal wind balance. By assuming cross-front thermal wind balance, forces acting on a parcel produce no transverse component of acceleration, but rather result in an instantaneous adjustment. Furthermore, accelerations in the along-front wind are constrained to thermodynamic changes through thermal wind balance. Thus, forces which accelerate fluid parcels on a time-scale less than the inertial time-scale cannot be accommodated within these 'balanced' theories.

The importance of diabatic processes on frontogenesis has long been recognised. Sawyer (1956) included in his study a parameterisation of reversible stable condensation, the latent heat being proportional to the vertical velocity. He found that the resultant diabatic warming locally increased the vertical velocity while decreasing the horizontal scale of the circulation, as well as enhancing frontogenesis near cloud base. Later balanced diagnostic investigations have also employed parameterisations of latent heat release by stable condensation (see e.g. Eliassen 1959; Rao 1966; and Emanuel 1985), as well as wave CISK parameterisations of penetrative convection, wherein the convective heating is proportional to the product of the low-level vertical velocity and a vertical structure function (see e.g. Mak and Bannon 1984; and Thorpe and Nash 1984). These, and more recent prognostic investigations of moist frontogenesis using numerical models (see e.g. Ross and Orlanski 1978; Williams et al. 1981; Hsie et al. 1984; and Thorpe and Emanuel 1985), have essentially reaffirmed Sawyer's conclusions. In the latter group, only Thorpe and Emanuel (1985) have imposed the balance assumptions discussed above.

Previous studies of surface cold fronts incorporating diabatic processes have almost exclusively concentrated on latent heat release. One exception, however, is the work of Pinkerton (1978), who investigated numerically the effects of differential sensible heating and friction on a frontal circulation forced by horizontal confluence. He found, as expected, that when the heat flux was prescribed to be greatest on the warm side of the front, the local scale of the frontal circulation contracted and its intensity increased.

Intense cold fronts regularly traverse southeastern Australia; their observed structure and evolution during the late spring and early summer months have been documented recently by Wilson and Stern (1985), Garratt et al. (1985), and Ryan and Wilson (1985). Generally, these fronts, known locally as 'cool changes', are orientated parallel to the southeastern South Australian coastline, which is predominantly northwest-southeast. Figure 1 shows a typical synoptic situation. Strong diurnal heating of the Australian continent produces large land-sea temperature contrasts normal to the front. While virga commonly accompanies the cool change, precipitation at the surface is observed in only about half of these fronts (Berson et al. 1957; Clarke 1961). Moreover, in contrast to its northern hemisphere counterpart, the prefrontal cloud base is generally high, typically about 700 hPa, reflecting the relative dryness of the cool change.

A deep, convectively well-mixed boundary layer frequently develops over the land during the spring and summer months. Thus, while moist diabatic processes may, to a first approximation, often be neglected, dry buoyant convection may play a significant role in the dynamics of the cool change through the vertical transport of sensible heat. Moreover, Berson et al. (1957), Clarke (1961), and Garratt et al. (1985) have all reported diurnal variations of frontal propagation speeds, the fronts usually accelerating and intensifying during the afternoon. Berson et al. (1957) and Garratt et al. (1985) have noted also a weak diurnal influence on the time at which fronts arrive at the coast; the cold air almost always crosses the coast during the daylight hours. In addition, the accompanying sea-breeze can at times be an integral component of the front-trough system over land (Clarke 1961; Garratt et al. 1985).

Reeder and Smith (1986, 1987) (hereafter referred to as RS86 and RS87, respectively) have argued that the dynamics and structure of cool changes are well represented by simple idealised two-dimensional numerical models of dry frontogenesis forced by horizontal shear. Here, the model described by RS87 is extended to include Dalu's (1978) parameterisation of dry buoyant convection driven by strong differential solar heating. The purpose of the present study is to assess the impact of dry buoyant convection on the cross-frontal circulation, and to provide a dynamical basis for understanding the role of land-sea temperature contrasts on the evolution of summertime cool changes as they approach and traverse the southern part of the Australian continent. In addition, the study aims to investigate the interaction of an idealised intense surface cold front, which is initially offshore, with a neutrally stable continental boundary layer, and to determine the importance of unbalanced frontogenesis associated with diabatic heating occurring on a diurnal time-scale.

The next section provides a brief outline of the equations and numerical model. Following that, the results of three numerical experiments are presented, while discussion of their dynamics and a comparison with observation is postponed until the succeeding section. The conclusion is given in the final section.

The basic equations and numerical model formulation

For this study, the two-dimensional numerical model described in RS87 is modified to include a parameterisation of differential diurnal heating representing a land-sea contrast. It is therefore appropriate to briefly outline the basic equations and numerical model formulation to be employed here.

Rectangular cartesian coordinates (x,y,z) are assumed with the x (zonal) coordinate normal to the front, the y (meridional) coordinate parallel to the front, and the z coordinate vertical. The Coriolis parameter, $f = -10^{-4}\ s^{-1}$, is taken to be negative so that the conventional coordinate orientation, with the y-axis pointing northward, can be used in the southern hemisphere context.

Assume the motion is composed of two parts: a time-independent zonally uniform geostrophic flow $(U_g(z), 0, 0)$ and a time-dependent deviation from this state with no meridional variation, $(u(x,z;t), v(x,z;t), w(x,z;t))$. Here, as in RS87,

$$U_g(z) = (U/H)z, \qquad \ldots 1$$

where $U = 60\ m\ s^{-1}$ and $H = 15\ km$ is the total depth of the flow. Thermal wind balance requires an associated time-independent potential temperature field of the form,

$$\Theta(y,z) = \Theta_o(z) - (f\Theta_{oo}U/gH)y, \qquad \ldots 2$$

where $\Theta_o(z)$ defines the vertical potential temperature structure (see RS87), $\Theta_{oo} = 316\ K$ is a reference

Fig. 1 Mean sea level isobaric analysis for a typical summertime situation in the Australian region. Prominent features are the surface cold front offshore and the prefrontal trough over southern Australia sandwiched between two anticyclones. Hot continental northerly flow precedes the front, with cooler maritime southwesterlies behind. (From Smith et al. 1982.)

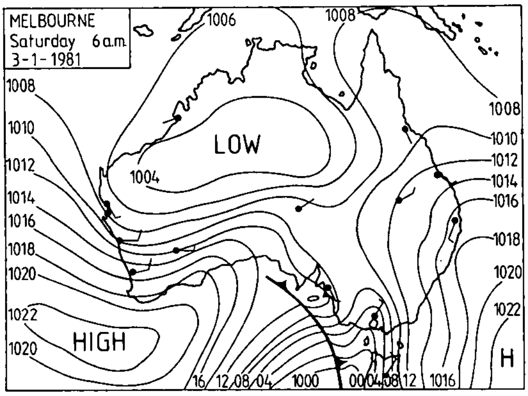

potential temperature, and $g = 9.81\,\mathrm{m\,s^{-2}}$ is the acceleration due to gravity. The lapse rate of basic state potential temperature, $d\Theta_o/dz$, is 4 K/km below the tropopause (at z = 10 km) and 15.5 K/km above.

The two-dimensional anelastic momentum, continuity, and thermodynamic equations are,

$$\frac{D}{Dt}(U_g + u) - fv = -\frac{\partial}{\partial x}\left(\frac{p}{\rho_o}\right) + K_M\frac{\partial^2 u}{\partial x^2}, \qquad \ldots 3a$$

$$\frac{Dv}{Dt} + fu = K_M\frac{\partial^2 v}{\partial x^2}, \qquad \ldots 3b$$

$$\frac{Dw}{Dt} - \frac{g(\Theta - \Theta)}{\Theta_{oo}} = -\frac{\partial}{\partial z}\left(\frac{p}{\rho_o}\right) + K_M\frac{\partial^2 w}{\partial x^2}, \qquad \ldots 3c$$

$$\frac{\partial u}{\partial x} + \frac{1}{\rho_o}\frac{\partial}{\partial z}(\rho_o w) = 0, \qquad \ldots 4$$

$$\frac{D\Theta}{Dt} = -v\frac{\partial \Theta}{\partial y} + \frac{\dot{Q}}{c_p\pi_e} + K_H\frac{\partial^2\Theta}{\partial x^2}, \qquad \ldots 5$$

where $D/Dt = \partial/\partial t + (U_g + u)\,\partial/\partial x + w\partial/\partial z$, p is the perturbation pressure, $\rho_o(z)$ is the basic state density as defined in RS87, $c_p = 1004\ \mathrm{J\,K^{-1}\,kg^{-1}}$ is the specific heat of dry air at constant pressure, $\pi_e = T/\Theta$ defines the Exner function with T being the temperature, and Q is the rate of diabatic heating per unit mass. Lateral mixing processes are explicitly included in the equations to maintain numerical stability. The horizontal diffusion coefficients for momentum and heat, K_M and K_H respectively, are constant and equal, with a value of $3 \times 10^4\ \mathrm{m^2\,s^{-1}}$.

Two-dimensionality allows the Eqns 3 to 5 to be conveniently re-expressed in a 'streamfunction-vorticity' form (see e.g. Orlanski and Ross 1977; RS86; and RS87). That is,

$$\frac{\partial \eta}{\partial t} - J\left(\psi, \frac{\eta}{\rho_o}\right) = f\frac{\partial v}{\partial z} - \frac{g}{\Theta_{oo}}\frac{\partial \Theta}{\partial x} + K_M\frac{\partial^2 \eta}{\partial x^2}, \qquad \ldots 6$$

$$\frac{\partial v}{\partial t} - \frac{J}{\rho_o}(\psi, v) = -\frac{f}{\rho_o}\frac{\partial \psi_a}{\partial z} + K_M\frac{\partial^2 v}{\partial x^2}, \qquad \ldots 7$$

and

$$\frac{\partial \Theta}{\partial t} - \frac{J}{\rho_o}(\psi, \Theta) = -v\frac{\partial \Theta}{\partial y} + \frac{\dot{Q}}{c_p\pi_e} + K_H\frac{\partial^2 \Theta}{\partial x^2}. \qquad \ldots 8$$

Here $J(a,b) = (\partial a/\partial x)(\partial b/\partial z) - (\partial a/\partial z)(\partial b/\partial x)$ is the Jacobian operator and the streamfunction, $\psi = \psi_a + \psi_g$, is defined by

$$(u,w) = \frac{1}{\rho_o}\left(\frac{\partial \psi_a}{\partial z}, -\frac{\partial \psi_a}{\partial x}\right), \qquad \ldots 9a$$

$$U_g = \frac{1}{\rho_o}\frac{d\psi_g}{dz}, \qquad \ldots 9b$$

where ψ_a and ψ_g represent the ageostrophic and geostrophic parts, respectively. Also, the meridional component of vorticity $\eta = \partial(U_g + u)/\partial z - \partial w/\partial x$ satisfies

$$\eta = \frac{1}{\rho_o}\frac{\partial^2 \psi}{\partial x^2} + \frac{\partial}{\partial z}\left(\frac{1}{\rho_o}\frac{\partial \psi}{\partial z}\right), \qquad \ldots 10a$$

which, under the hydrostatic assumption, reduces to

$$\eta = \frac{\partial}{\partial z}\left(\frac{1}{\rho_o}\frac{\partial \psi}{\partial z}\right). \qquad \ldots 10b$$

Dry buoyant convection over the land, due to diurnal heating, is incorporated through the diabatic heating term in Eqn 8, $\dot{Q}$, and is parameterised by a simple convective adjustment scheme proposed by Dalu (1978). The temporal variation of $\dot{Q}$, is given by a sine function with a period of one day which roughly models the diurnal heating cycle. The coastline is located at the origin with the sea to the left (west) and the land to the right (east). It is assumed that the lower boundary is smooth and that there is no sensible heat exchange with the sea. While only horizontal diffusion processes are explicitly incorporated into the model (see Eqns 6 to 10), vertical mixing of heat is implicit in the parameterisation of buoyant convection. Upright convective mixing in the model occurs only when vertical temperature gradients at the surface become (absolutely) unstable (for details, see Appendix). In this parameterisation heat convection is assumed inefficient in mixing momentum. Dalu (1978) demonstrated that the parameterisation produced a sea-breeze which compared well both with observation and more sophisticated numerical models. Moreover, in a numerical study of differential boundary layer development across a dryline, Sun and Ogura (1979) concluded that the vertical mixing of heat was of far greater dynamical importance than the vertical mixing of momentum.

Although Dalu's (1978) convective parameterisation does not include surface friction effects, it is both computationally inexpensive and conceptually straightforward. More importantly, it is intermediate in sophistication between those used in simple analytic studies and those used in more detailed mesoscale models with complex physical parameterisations. As such, incorporation of Dalu's (1978) scheme into the model of RS87 provides a conceptual framework for further theoretical and observational investigations.

Equations 6, 7, 8, and 10 are transformed using a stretched vertical coordinate to increase resolution near the ground (see RS87), and approximated by the finite difference analogues described in RS86, that is, central differences in space together with the explicit time-differencing scheme of Miller and Pearce (1974). The time-step, Δt, is 60s. The lateral boundary conditions are open (Miller and Thorpe 1981), while the top and bottom boundary conditions assume no-stress and zero vertical velocity (see RS87).

Numerical simulation of a differentially heated surface cold front demands adequate resolution of a broad spectrum of horizontal length scales, from at least the scale of the cross-front ageostrophic frontal circulation (i.e. the Rossby radius of deformation) down to the scale of the sea-breeze. Using the nomenclature of Orlanski (1975), the resolution must encompass the meso-α (200 to 2000km) to the meso-γ (2 to 20km) scale. The computational domain of integration extends horizontally from $x = -1648$km to $x = 2852$km (a total length of 4500km) and in the vertical from $z = 0$ to $z = H$, with a horizontal grid length of $\Delta x = 16$km and a vertical grid length of between $\Delta z = 120$m near the ground and 800m near the top boundary.

While the numerical solutions presented herein are calculated without assuming hydrostatic balance, comparison with hydrostatic solutions of the same cases reveals the results to be almost imperceptibly different. This is to be expected since the ratio of horizontal to vertical scales resolvable by the model is large ($\Delta x/\Delta z \sim 133$). The ratio of horizontal and vertical grid sizes is chosen so as to be consistent with the slope of the front.

Results

Three numerical experiments are now presented. The first, hereafter referred to as SB, assesses the response of the model to differential diurnal heating in the absence of a synoptic surface front; it is therefore essentially a study of sea-breeze development in a sheared environment. The second, F, investigates the behaviour of an idealised surface cold front when diabatic heating is neglected. Finally, FD combines the aforementioned numerical experiments to probe the dynamics of a surface cold front interacting with a prefrontal well-mixed layer formed by differential diurnal heating. The first two numerical experiments act as controls for the latter model run.

The initial conditions for F and FD are those used by RS87 and represent an idealised cross-section through a typical pre-existing, finite-amplitude disturbance prior to its amplification into an intense front-trough system. In brief, the initial state consists of a zonal shear flow in thermal wind balance (Eqns 1 and 2) in which is embedded a warm prefrontal northerly airstream, $v(x,z;0)$ (for details of the form of $v(x,z;0)$, see RS87). As shown by RS87, the front-trough system reaches a quasi-steady state after about six hours (see also Fig. 9 later in this section). For simplicity, the diurnal heating cycle in FD is started after six hours of model integration and thereafter is continued for a further twelve hours. Both F and FD are therefore integrated a total of eighteen model hours. At the commencement of the diurnal heating cycle, the surface cold front is chosen, somewhat arbitrarily, to be 224km offshore, which results in the front propagating onshore in the early afternoon when the low-level mixed layer is well established.

The initial conditions for SB consist solely of a zonal shear flow in thermal wind balance (Eqns 1 and 2). In contrast, previous sea-breeze studies, with the exception of Sun and Ogura (1979), have assumed a barotropic initial state. The diurnal heating cycle begins at the initial instant and continues for twelve hours.

Although the domain of integration has a total horizontal length of 4500km and a vertical extent of 15km, attention will be focused on the low-level features of the front-trough system in the neighbourhood of the coastline. Accordingly, all model x-z cross-sections presented will be confined to the subdomain extending 320km both upstream and downstream from the coastline and from the ground to a height of 4.2km.

SB

As the continental air is heated, it expands hydrostatically. The mass field adjusts through divergence aloft, resulting in a surface pressure fall over the continent and accompanying onshore flow

Fig. 2 Perturbation streamfunction, ψ_a (dashed contours), and potential temperature, θ (solid contours), at t = 9 hours for SB. Contour intervals are 200 kg m s^{-1} and 1 K. The arrowheads indicate the sense of the circulation.

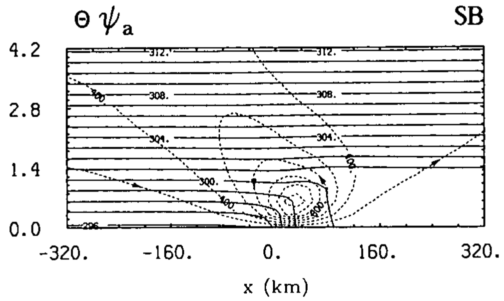

near the ground. Figure 2 displays the perturbation streamline pattern, ψ_a, in x-z cross-section, superposed on the isentropes, θ, after nine hours of integration. The single-cell circulation is thermally direct and exhibits a well-developed low-level onshore airstream with upper-level return flow. At this time, the zonal perturbation velocity, u, has attained its maximum value, 4 m s^{-} , at a point 24 km inland from the coast.

A prominent feature of the potential temperature pattern is the development of a well-mixed layer over the continent which deepens uniformly with time, attaining a depth of 1.4 km after nine hours of heating (Fig. 2). After six hours, the model exhibits a horizontal potential temperature gradient ($\partial\theta/\partial x$) of 0.6 K/10 km near the coast. Although the surface heat flux wanes after six hours, the maximum temperature gradient, 0.7 K/10 km, is achieved approximately two hours later due to nonlinear 'sharpening' by the ageostrophic circulation. Subsequently, onshore advection of cooler maritime air, in addition to lateral diffusion, weakens the coastal temperature gradient and advects the coastal baroclinic zone inland. Figure 2 exhibits a weak baroclinic zone extending some 80 km inland, the temperature difference across the baroclinic zone being 3.5 K.

Fig. 3 Vertical velocity, w, at t = 9 hours for SB. Dashed contours denote negative values. Contour interval is 0.2 cm s^{-1}.

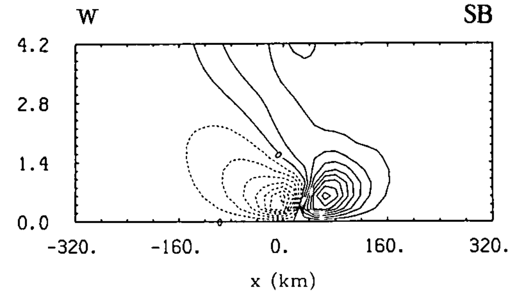

Isotachs of vertical velocity, w, after nine hours of integration are presented in Fig. 3. The maximum ascent, which develops concomitantly with the surface convergence maximum, attains its peak value about one hour earlier. The maximum upward motion at t = 9 hours, 1.7 cm s^{-1}, is located 65 km inland, whereas the maximum subsidence, -1.5 cm s^{-1}, occurs at the coast. The maximum convergence at this time ($-\partial u/\partial x$) is 4.7×10^{-5} s^{-1}.

Figure 4 displays the zonal variation of the total meridional velocity v, and the geostrophic meridional velocity $v_g \equiv (\rho_0 f)^{-1}\, \partial p/\partial x$ at a height of z = 120 m, after nine hours of integration. Since the numerical solution remains close to hydrostatic balance, the buoyancy is at all times directly coupled to the pressure [i.e. $\partial(p/\rho_0)/\partial z = g(\theta - \Theta)/\theta_{00}$]. At this time, the amplitude and phase of v and v_g are nearly equal. Note that v_g is nonzero some 100 km offshore, indicating that upstream maritime air parcels 'feel' the differential diabatic heating through the agency of the pressure field before reaching the coastline. Indeed, low-level air parcels must begin their acceleration upstream of the coast if they are to reach the shore with a zonal velocity in excess of U_g (see Fig. 2). Subsequent Coriolis turning of the resultant low-level ageostrophic zonal circulation produces low-level southerlies (Fig. 4). Prior to about nine hours, the total meridional wind is sub-geostrophic, thereafter becoming supergeostrophic.

While comparison of the numerical solution presented here with observational, analytic, and previous numerical studies shows reasonable agreement (see e.g. Dalu 1978; Sun and Ogura 1979; Atkinson 1981; and Rotunno 1983), the model simulation represents a rather broad weak sea-breeze circulation and baroclinic zone, due in part to the model's relatively coarse resolution and high static stability. In addition, a strong onshore geostrophic wind, as in the model, does not favour the formation of the sea-breeze (see Atkinson 1981). Comparison of SB with a sea-breeze simulation with a barotropic basis state (not presented here) shows differential meridional temperature advection to be insignificant in the formation of the coastal baroclinic zone.

F and FD

Figure 5(a) displays an x-z cross-section of the perturbation streamlines and isentropes for F after fifteen hours of model integration, while Fig. 5(b) shows the equivalent cross-section for FD. At this time, the latter model run has undergone nine hours of diurnal heating. Both numerical solutions exhibit a thermally direct two-cell circulation pattern with low-level convergence. While both circulation patterns show broadscale agreement, there remain highly significant differences. In particular, Fig. 5(b) displays a more upright streamline pattern just ahead of the cold air together with an increase in the low-level convergence.

Fig. 4 Zonal variation of geostrophic meridional velocity, v_g (solid line), and total meridional velocity, v (dashed line), for SB at a height of z = 120 m after 9 hours. v and v_g have units of m s^{-1}.

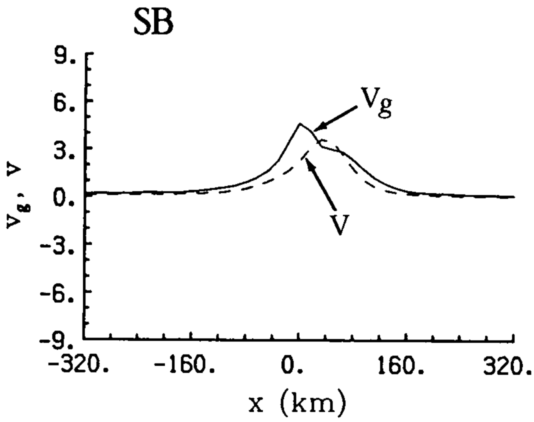

Fig. 5 Perturbation streamfunction, ψ_a (dashed contours), and potential temperature, θ (solid contours), at t = 15 hours for (a) F and (b) FD. Contour intervals are 3x10^3 kg m s^{-1} and 3K. The arrowheads indicate the sense of the circulation. The thick solid line shows the height of the well-mixed layer.

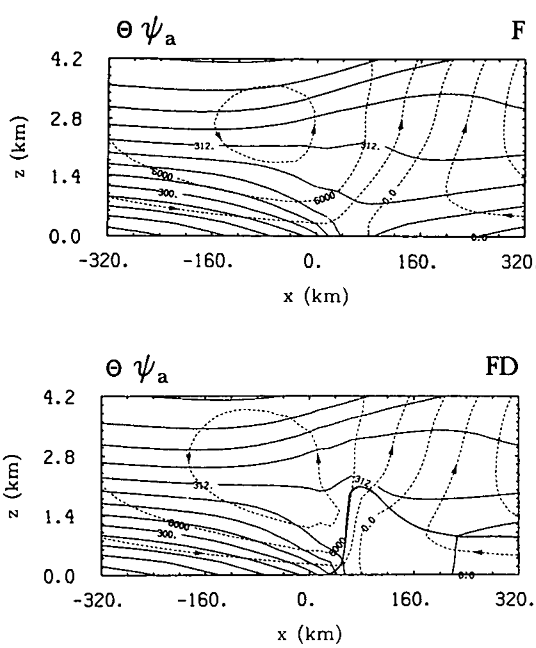

At this time, the front, defined as the point of maximum surface temperature gradient, is located at x = -12 km for F and x = 41 km for FD. The heavy solid line in Fig. 5(b) indicates the height of the mixed layer, which attains its greatest depth immediately ahead of the front. Note also that the maximum temperature is located just ahead of the surface front for both F and FD. Diurnal heating has increased the prefrontal surface temperatures by about 6 K. As the front propagates inland, a shallow layer of cold postfrontal air is advected onshore and greatly modifies the height of the mixed layer between the coast and about x = 55 km.

Differences in the circulation patterns between the two cases are dramatically highlighted in the x-z cross-sections of the vertical velocity isotachs, again displayed at fifteen hours (Fig. 6). FD has developed an intense narrow updraft with a maximum of 24 cm s^{-1}, its centre being located about 63 km inland and 1.2 km above the ground. In contrast, F exhibits a vertical velocity maximum of only 7 cm s^{-1}. Clearly, the FD circulation cannot be interpreted as a linear sum of the SB and F circulations, since the vertical velocity maximum for SB, after nine hours of diurnal heating, was only 1.7 cm s^{-1} (see Fig. 3). The dynamics of this synergism will be discussed in the next section. Both F and FD exhibit subsidence rates of about 1-2 cm s^{-1} in the cold postfrontal air. Referring back to Fig. 5(b), a cold dome, associated with differential vertical advection by the intense updraft, is evident in the isentropes.

Fig. 6 Vertical velocity, w, at t = 15 hours for (a) F and (b) FD. Dashed contours denote negative values. Contour interval is 2 cm s^{-1}.

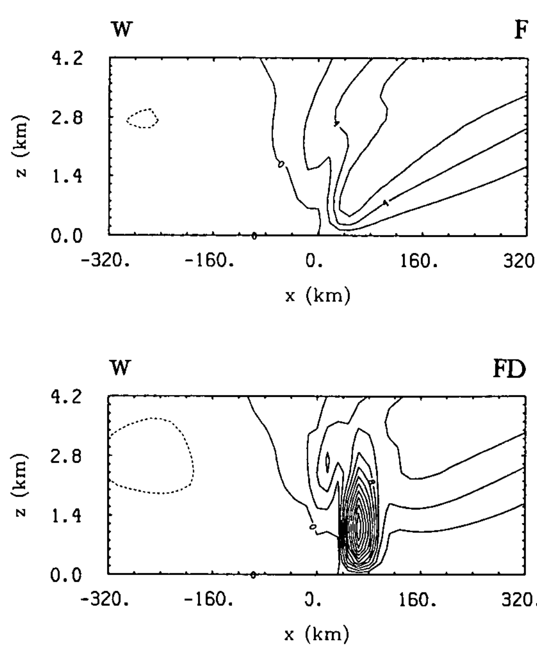

The zonal variation of the total meridional velocity and the geostrophic meridional velocity, at a height of 120 m, for F and FD are displayed in Figs 7(a) and 7(b), respectively. As before, the graphs are presented after fifteen hours of integration. Both F and FD exhibit post-frontal southerlies and northerlies far ahead of the front ($x \geq 400$ km) which are very nearly in geostrophic balance. In the neighbourhood of the front and in the immediate prefrontal region ($x \leq 400$ km) however, both numerical solutions display pronounced ageostrophic meridional motions. Recall that the initial meridional airflow was strictly northerly. As discussed in RS87, the postfrontal southerlies developed during the integration period due to Coriolis turning of the ageostrophic zonal circulation. Figure 7(b) displays a large increase in the along-front geostrophic wind in the region between $x = 40$ km and $x = 120$ km, reflecting the decrease in cross-front pressure gradient associated with the diurnal heating.

Fig. 7 Zonal variation of geostrophic meridional velocity, v_g (solid line), and total meridional velocity, v (dashed line), for (a) F and (b) FD at a height z = 120 m after 15 hours.

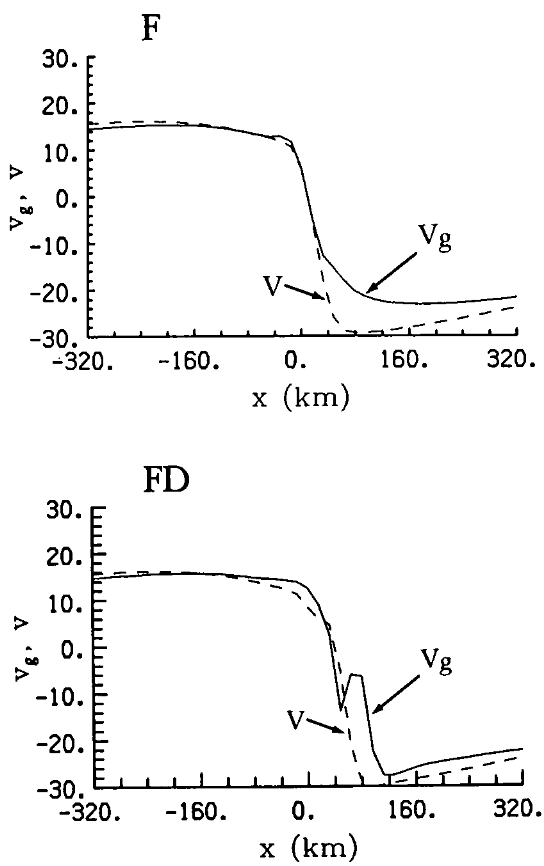

The zonal variation of the vertical component of vorticity, convergence, and horizontal potential temperature gradient, calculated at 120m above the surface after fifteen hours of integration, are displayed in Figs 8(a) and 8(b) for F and FD respectively. At this time, the cyclonic vorticity, convergence, and horizontal potential temperature gradient for F have maximum values of $7 \times 10^{-4}s^{-1}$, $17 \times 10^{-5}s^{-1}$, and 1.7 (K/10km), whereas the corresponding quantities for FD are $8 \times 10^{-4}s^{-1}$, $42 \times 10^{-5}s^{-1}$, and 2.3 (K/10km). Comparison of Figs 8(a) and 8(b) discloses the surface front in the latter to be located roughly 30 km further inland, indicating a weak acceleration in the presence of heating. For F, the frontal speed at this time is 8.3 m s^{-1}, while for FD it is 9.6ms^{-1}.

Fig. 8 Zonal variation of vertical vorticity, ζ (solid line), horizontal divergence, $\partial u/\partial x$ (dashed line), and horizontal temperature gradient, $\partial\theta/\partial x$ (short/long dashed line), for (a) F and (b) FD at a height z = 120 m after 15 hours. ζ, $\partial u/\partial x$, and $\partial\theta/\partial x$ have units of $10^{-4}s^{-1}$, $10^{-5}s^{-1}$, and K (10km)$^{-1}$, respectively.

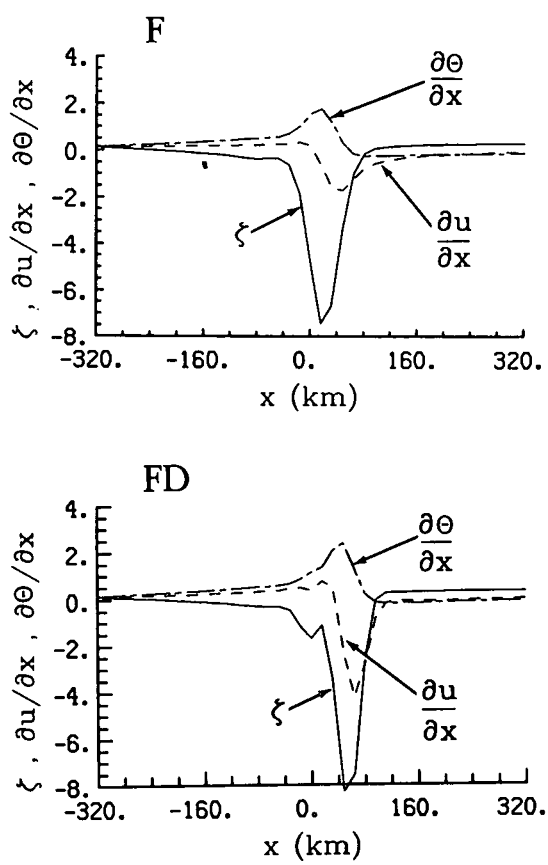

A good overview of the temporal variation of the numerical solutions for F and FD can be gained by inspecting the time series of vorticity, convergence, and horizontal potential temperature gradient maxima at z = 120m (see Fig. 9). Prior to the commencement of diurnal heating, both solutions are identical. A striking feature of the convergence time series for FD is the very rapid rise between t = 12 and t = 16 hours accompanying the development of the intense prefrontal updraft (see Figs 9(b) and 6(b)). Note also that the maximum convergence decreases relative to F shortly after the heating begins. This is because the front, and its associated convergence maximum, are at this time offshore in a region where the sea-breeze circulation is divergent. Subsequently, convergence development precedes vorticity development by roughly one and a half hours. Rapid frontogenesis is clearly evident in the potential temperature gradient time series for FD.

Fig. 9 **Time series of maxima of (a) vertical vorticity, ζ, in $10^{-4}s^{-1}$, (b) horizontal convergence, $-\partial u/\partial x$, in $10^{-5}s^{-2}$, and (c) horizontal temperature gradient in $(100km)^{-1}$ at a height z = 120 m for F (solid lines) and FD (dashed lines).**

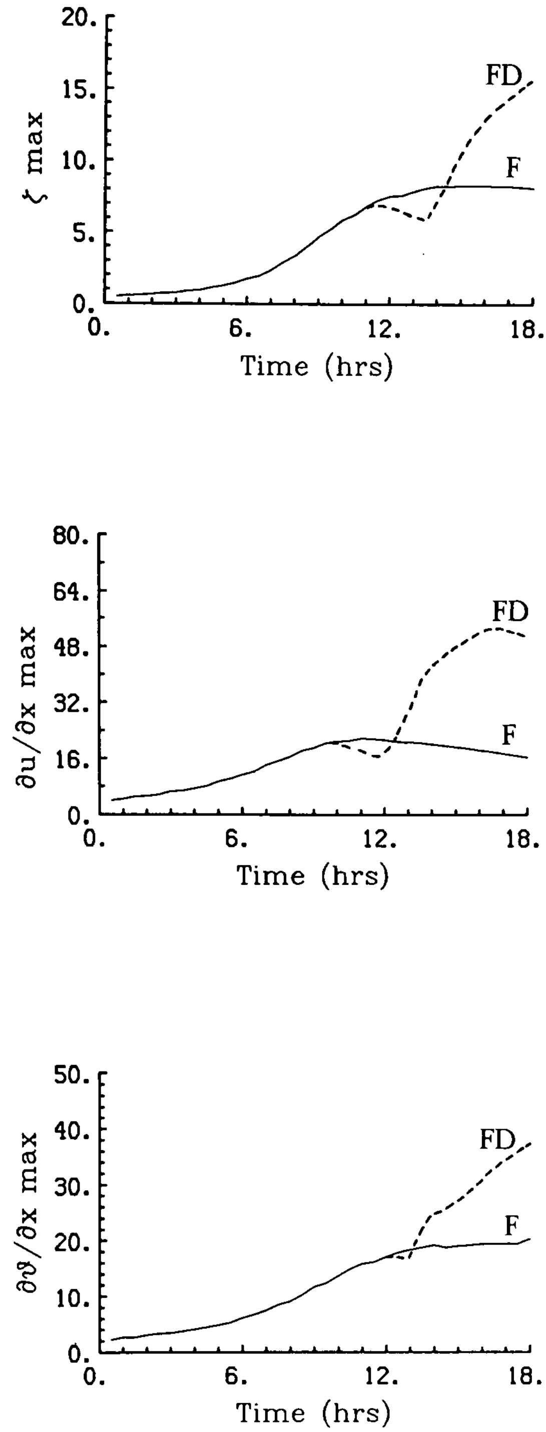

Discussion of results and comparison with observation

As shown in the previous section, the interaction of an idealised front with a well-mixed layer resulted in a sharp increase in prefrontal convergence and associated vertical velocity which could not be attributed soley to the sea-breeze circulation. In addition, the numerical solution exhibited rapid frontogenesis and a weak frontal acceleration.

Before proceeding, the possible role of symmetric instability is investigated. On the basis of viscous linear theory and a Prandtl number of unity or inviscid linear theory, a necessary condition for the onset of dry symmetrically unstable overturning is that

$$\Delta = [(1 + f^{-1}\,\partial v_g/\partial x)g/\Theta_{oo}(\partial\Theta/\partial z) - (\partial v_g/\partial z)^2] < 0$$

(See e.g. Hoskins 1974).* The most unstable modes are manifest as rolls oriented parallel to the vertical geostrophic wind shear within the layer of symmetric instability, with the transverse motion approximately parallel to the isentropes. After about fifteen hours of model integration, FD has developed a region in the prefrontal mixed layer where Δ is negative. To assess whether the intense updraft which developed in FD is in fact a result of symmetric instability, a similar procedure to that first described by Orlanski and Ross (1977) is used. The fifteen-hour potential temperature and meridional velocity fields are used as initial conditions for an experiment where $\psi = U_g = 0$ and no further heat is added. If symmetric instability were a factor, the intense updraft would be expected to quickly reform; it does not.

*Note that $\Delta < 0$ is not equivalent to $q < 0$, where $q = [(1 + f^{-1}\,\partial v_g/\partial x)g/\Theta_{oo} - (\partial u_g/\partial z)^2 - (\partial v_g/\partial z)^2]$ is the geostrophic Ertel potential vorticity. Using Eqn 1, $q = \Delta - U^2/H^2$.

Nonlinear interaction between the diurnal heating and the frontal circulation is now explored. As discussed earlier, differential changes in the buoyancy are coupled through near hydrostatic balance to instantaneous adjustments in the geostrophic meridional wind. However, no such constraint is imposed on the total meridional wind, which changes more slowly due to inertia. Indeed, comparison of Figs 7(a) and 7(b) shows the total meridional wind to have changed little in F and FD. Therefore, increases in the geostrophic wind are accompanied by an almost equivalent decrease in the ageostrophic meridional wind, $v_a \equiv v - v_g$. The inviscid form of Eqn 3(a), namely $D(U_g + u)/Dt = fv_a$, indicates that fluid parcels are (positively) accelerated in regions of negative ageostrophic meridional wind (recall $f<0$). Immediately ahead of the front, the cross-front acceleration is enhanced in FD due to the relatively large decrease in ageostrophic meridional velocity associated with the diurnal heating (see Fig. 7). Moreover, it is worth noting that the inviscid form of Eqn 6, which may be written as $D\eta/Dt = f\partial v_a/\partial z$, points to a lack of cross-front thermal wind balance as the (inviscid) source of meridional vorticity and associated zonal circulation.

Consider now the convergence equation,

$$\underset{\mathrm{I}}{\frac{D}{Dt}\left(-\frac{\partial u}{\partial x}\right)} = \underset{\mathrm{II}}{\left(\frac{\partial u}{\partial x}\right)^2} \underset{\mathrm{III}}{- f\frac{\partial v_a}{\partial x}} + \underset{\mathrm{IV}}{\frac{\partial w}{\partial x}\frac{\partial u}{\partial z}} + \underset{\mathrm{V}}{K_M\frac{\partial^2}{\partial x^2}\left(-\frac{\partial u}{\partial x}\right)}, \quad \ldots 11$$

obtained by taking the x-derivative of Eqn 3(a). For F and FD, the maximum rates of increase of convergence following a fluid parcel (term I) after fifteen hours are located approximately 60 and 90 km inland from the coast, respectively. Table 1 lists the value of each term at this point, calculated 120 m above the ground. Inspection of the table shows term II to be the most dominant term in Eqn 11 for both F and FD. Each term is five times larger in FD than F. Term III, the ageostrophic meridional velocity term, couples the convergence explicitly to changes in the pressure field, the convergence increasing in regions of anticyclonic vorticity (see Fig. 7). Term II, the quadratic term, produces convergence in areas of pre-existing convergence (or divergence) and gives the largest contribution to the nonlinear amplification of the circulation in FD.

Comparison of the vertical velocity predicted by FD (Fig. 6(b)) with observation (Garratt et al. 1985) shows substantial agreement. However, it should be remembered that RS86 were able to explain the observed intense prefrontal updraft in terms of boundary layer convergence. Nevertheless, it is likely that both diabatic and frictional mechanisms are important in its development. Clarke (1961) has reported an observed preference for prefrontal squall lines to develop in the late afternoon. Interestingly, the intense updraft formed in FD also reaches a maximum late in the afternoon. This suggests perhaps a *prima facie* case for the diabatically enhanced low-level circulation providing a favorable environment for late afternoon prefrontal convection. Destabilisation of the prefrontal boundary layer in concert with local intensification of the prefrontal updraft, both due to diurnal heating, may have the capacity to lift potentially unstable air parcels to their level of free convection. Moreover, squall lines initiated by the cross-front frontal circulation would, as observed, be aligned parallel to the front (Garratt et al. 1985).

Koch (1984) has documented recently the explosive development of a band of severe thunderstorms from a narrow line of shallow convection in a region of rapid frontogenesis. He presents evidence of differential boundary layer development and explains the storms' initiation through an inferred associated mesoscale circulation (an 'inland sea breeze'; see Sun and Ogura 1979), which is consistent with the present study.

The weak diurnal variation of the predicted frontal speed in FD is in agreement with observation (see e.g. Berson et al. 1957; Clarke 1961; and Garratt et al. 1985). In F, the surface front reaches the coastline at t = 14½ hours, whereas in FD it arrives about one hour earlier (i.e. about 7½ hours after the commencement of diurnal heating). As the front encounters the well-mixed continental boundary layer in the latter run, two mechanisms act to accelerate the front. Firstly, as argued previously, diurnal heating serves to increase the convergence ahead of the front, leading to the development of a second surface temperature gradient maximum. This results in *in situ* frontogenesis near the coast in advance of the pre-existing front. Secondly, rapid frontogenesis leads to a contraction of the frontal zone; the position of the front advances toward the

Table 1. Contributions to the convergence equation calculated at the point of maximum increase in convergence following a fluid parcel, at z = 120m and after 15 hours of integration. Units are $10^{-7}s^{-2}$.

	I	II	III	IV	V
F	1.8	1.5	0.5	-0.2	2×10^{-5}
FD	9.4	7.7	2.6	-0.9	3×10^{-6}

position of maximum convergence. In F, their separation distance was 39 km, whereas in FD it was only 21 km. While observational data on the evolution in structure of the cool change is somewhat fragmentary, there is supporting evidence for rapid frontogenesis as the front propagates onshore (Clarke 1961; Smith et al. 1982; Garratt et al. 1985; Garratt and Physick 1986).

Recent observations of the mesoscale structure of cool changes in the late spring and early summer months have revealed substantial front-relative flow through the front from warm to cold air (Reeder et al. 1982; Garratt et al. 1985). That is, the front moves faster than the normal component of the low-level wind, and therefore, in some sense, propagates. In addition, it has been shown that the low-level structure includes a broad but shallow baroclinic zone (~200 km wide and ~2 km deep), known as the frontal transition zone, in which may be embedded several lines of change at the surface, these usually being associated with prefrontal squall lines. The final change line, which is analysed as the cold front and generally shows most continuity as the system evolves, is associated with a zone of enhanced baroclinicity some 2 or 3 km deep.† RS86 and RS87 have numerically modelled the dynamics of dry cool changes with the above characteristics. In contrast, Clarke (1961) and Garratt and Physick (1986) have published observational evidence of a second class of mid and late summertime cold fronts with a single well-defined change line without a complex frontal transition zone, and a low-level structure which is locally similar to a gravity current. Moreover, the low-level flow immediately behind the front is faster than the speed of the front; thus, these fronts appear to be advected.

Figures 10(a) and 10(b) show x-z cross-sections of the relative streamlines, $\psi_r = \int_0^z \rho_0 (u - c)\, dz$, for F and FD respectively, after fifteen hours of integration; here, c is the speed of the front. In the former numerical experiment, the relative flow is clearly through the frontal surface towards colder air, whereas in the latter run a region of closed recirculating flow has developed behind the front. Comparison of Fig. 10(b) with the observed streamline analyses presented by Clarke (1961) and Garratt and Physick (1986) shows close agreement. Similarly, Fig. 10(a) agrees well with the observed cross-front velocity fields reported by Reeder et al. (1982) and Garratt et al. (1985). Insofar as the front may be considered steady, the relative streamlines shown in Fig. 10 may be taken to be parcel trajectories. Interestingly, air moving through the intense prefrontal updraft in Fig. 10(b) originates in the well-mixed continental boundary layer ahead of the front. Thus, the development of an associated squall line, as hypothesised earlier, may be closely tied to the availability of moisture in the prefrontal boundary layer.

The relationship between synoptic-scale fronts and gravity currents, and the circumstances under which fronts develop gravity-current-like features, is not at all well understood (Smith and Reeder 1986). Nevertheless, the present study hints at a mechanism which may help explain the formation of gravity-current-like fronts from synoptic-scale fronts. The importance of prefrontal diabatic heating and stratification on both the intensity and lateral scale of the cross-front ageostrophic circulation is clearly evident from the numerical experiments reported herein. As the prefrontal air is heated, large cross-front parcel accelerations and rapid *in situ* frontogenesis lead to a scale contraction which may hypothetically culminate in a locally gravity-current-like frontal structure. Indeed, observation shows that the prefrontal northerlies ahead of the two gravity-current-like fronts reported by Garratt and Physick (1986) were excessively hot and the convectively well-mixed layer reached a height greater than 2 km. Of course, the above hypothesis, together with the importance of associated moist convection and evaporative cooling, requires further investigation.

Fig. 10 Relative streamfunction, ψ_r, at t = 15 hours for (a) F and (b) FD. Contour interval is 10^3 kg m s^{-1}. The arrowheads indicate the sense of the circulation.

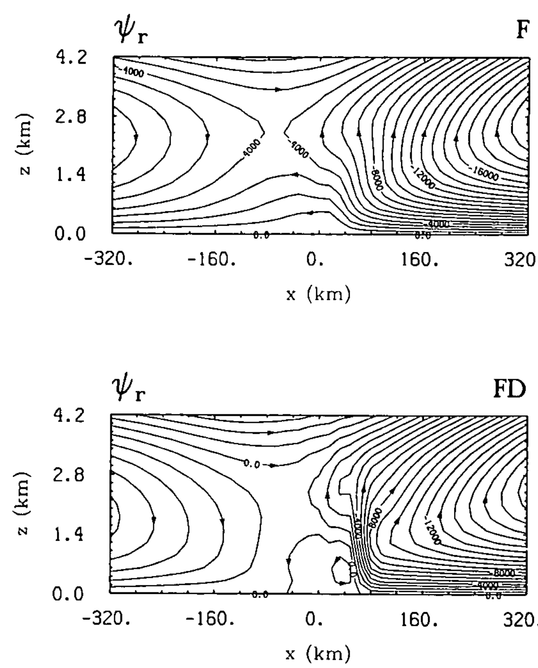

†In situations of strong prefrontal moist convection, the surface position of the final line may be greatly obscured by low-level evaporative cooling.

Conclusions

Reeder and Smith (1987) investigated the dynamics of the Australian summertime cool change using a two-dimensional dry anelastic streamfunction vorticity model. In the present study, the model is extended to incorporate a simple parameterisation of dry buoyant convection driven by diurnal heating. The parameterisation assumes a smooth lower boundary and that the convective mixing redistributes the added heat uniformly in the vertical, forming a thermodynamically well-mixed continental boundary layer. While surface friction is undoubtedly important in determining the details of the low-level structure, the study aims to investigate the effects of dry buoyant convection alone on the cross-front circulation, and thus provide a simple conceptual framework for further work. The study provides a natural bridge between simple analytic theory and more complex mesoscale models with sophisticated physical parameterisations.

Three numerical experiments are discussed. The first, SB, assesses the model's response to differential diurnal heating in the absence of a front, and is therefore essentially a study of sea-breeze development in a sheared environment. The second, F, investigates the dynamics of the cool change without diurnal heating and, as such, recapitulates the work of Reeder and Smith (1987). The final numerical experiment, FD, adds differential diurnal heating to the second experiment with the coastline 224 km ahead of the front at the commencement of the heating cycle.

The effect of diurnal heating on the cross-front frontal circulation is shown to be profound, but localised. In particular, an intense prefrontal updraft develops late in the afternoon in response to the heating. Moreover, the frontal structure and circulation modified by heating, FD, cannot be interpreted as a linear superposition of the frontal solution without heating, F, and the sea-breeze solution, SB, but rather, can be associated with the quadratic convergence term in the convergence equation (Eqn 11). Additional responses to the imposed heating are a sharp increase in cyclonic vorticity, rapid unbalanced frontogenesis, and an accompanying weak frontal acceleration.

Diurnal heating acts to increase the horizontal temperature gradient and to decrease the static stability. In doing so, a necessary condition for symmetric instability based on linear Boussinesq theory is violated within the mixed layer, i.e. $\Delta < 0$. Nevertheless, the numerical simulations, which employ the viscous nonlinear anelastic equations, remain symmetrically stable. This, and the relatively large transverse parcel accelerations, precludes analysis of the dynamics of FD in terms of well-established 'balanced' frontal theories (e.g. Sawyer 1956; Eliassen 1959, 1962; and Hoskins and Bretherton 1972).

While the numerical solutions presented are consistent with observation, the existing data are insufficiently well resolved in time and space to confidently substantiate the model's predictions. Nevertheless, the model provides a theoretical and conceptual framework in which much of the diurnal variation of cool changes may be explained. The model hints at an intriguing mechanism whereby synoptic-scale fronts may rapidly intensify, forming gravity-current-like features, and thus provide a possible unifying explanation for the two disparate classes of frontal structure reported by (i) Reeder et al. (1982) and Garratt et al. (1985) and (ii) Berson et al. (1957), Clarke (1961), and Garratt and Physick (1986). In particular, the inclusion of diurnal heating leads to the formation of a region of closed front-relative flow behind the front (Fig. 10) as reported by the second group of authors. This hypothesis, including a more precise and practical criterion for the onset of rapid diabatic frontogenesis, needs further investigation. In addition, the extent to which this hypothesised mechanism contributes to the generation of the Southerly Buster should be studied also.

Acknowledgments

This work was initiated at the Geophysical Fluid Dynamics Laboratory, Monash University, Australia, and later completed at the Laboratory for Atmospheres, NASA/Goddard Space Flight Center, USA. I am grateful to Roger Smith of Monash University, and Dan Keyser and Steve Koch of NASA/Goddard for their interest and constructive suggestions. Thanks are due also to Kelly Wilson for typing the manuscript.

References

Atkinson, B.W. 1981. *Meso-scale Atmospheric Circulations.* Academic Press, 495 pp.

Berson, F.A., Reid, D.G. and Troup, A.J. 1957. The summer cool change of southeastern Australia. I: General behaviour. *Tech. Pap. No. 8*, CSIRO Div. of Met. Phys., Mordialloc, Australia. 48 pp.

Clarke, R.H. 1961. Mesoscale structure of dry cold fronts over featureless terrain. *J. Meteor., 18*, 715-35.

Dalu, G.A. 1978. A parameterisation of heat convection for a numerical sea breeze model. *Q. Jl R. met. Soc., 104*, 797-807.

Eliassen, A. 1959. On the formation of fronts in the atmosphere. *The Atmosphere and Sea in Motion.* Rockefeller Institute Press, New York, 277-87.

Eliassen, A. 1962. On the vertical circulation in frontal zones. *Geofys. Publikasjoner, 24(4)*, 147-60.

Emanuel, K.A. 1985. Frontal circulations in the presence of small moist symmetric stability. *J. Atmos., Sci., 42*, 1062-71.

Garratt, J.R. and Physick, W.L. 1986. Numerical study of atmospheric gravity currents. I: Simulations and observations of cold fronts. *Beitr. Phys. Atmos., 59*, 282-300.

Garratt, J.R., Physick, W.L., Troup, A.J. and Smith, R.K. 1985. The Australian summertime cool change. II: Mesoscale aspects. *Mon. Weath. Rev., 113*, 202-23.

Hoskins, B.J. 1974. The role of potential vorticity in symmetric stability and instability. *Q. Jl R. met. Soc., 100*, 480-82.

Hoskins, B.J. and Bretherton, F.P. 1972. Atmospheric frontogenesis models: Mathematical formulation and solution. *J. Atmos. Sci., 29*, 11-37.

Hsie, E.-Y., Anthes, R.A. and Keyser, D. 1984. Numerical simulation of frontogenesis in a moist atmosphere. *J. Atmos. Sci., 39*, 1783-802.
Koch, S.E. 1984. The role of an apparent mesoscale frontogenetic circulation in squall line initiation. *Mon. Weath. Rev., 112*, 2090-111.
Mak, M. and Bannon, P.B. 1984. Frontogenesis in a moist semi-geostrophic model. *J. Atmos. Sci., 41*, 3485-500.
Miller, M.J. and Pearce, R.P. 1974. A three-dimensional primitive equation model of cumulonimbus convection. *Q. Jl R. met. Soc., 100*, 133-54.
Miller, M.J. and Thorpe, A.J. 1981. Radiation conditions for the lateral boundaries of limited-area models. *Q. Jl R. met. Soc., 107*, 615-28.
Orlanski, I. 1975. A rational subdivision of scales for atmospheric processes. *Bull. Am. met. Soc., 56*, 527-30.
Orlanski, I. and Ross, B.B. 1977. The circulation associated with a cold front. Part I: Dry case. *J. Atmos. Sci., 34*, 1619-33.
Pinkerton, J.E. 1978. Numerical experiments on boundary layer effects on frontal structure. Ph.D. Thesis, Drexel University, Philadelphia, PA 19104, 213 pp.
Rao, G.V. 1966. On the influences of fields of motion, baroclinicity and latent heat sources on frontogenesis. *Jnl appl. Met., 5*, 377-387.
Reeder, M.J., Roff, G., Smith, R.K., Garratt, J.R. and Reid, D.G. 1982. Low-level winds. *Tech. Report 51*, Bur. Met., Australia, 41-6.
Reeder, M.J. and Smith, R.K. 1986 (RS86). A comparison between frontogenesis in the two-dimensional Eady model of baroclinic instability and summertime cold fronts in the Australian region. *Q. Jl R. met. Soc., 112*, 293-313.
Reeder, M.J. and Smith, R.K. 1987 (RS87). A study of frontal dynamics with application to the Australian summertime 'cool change'. *J. Atmos. Sci., 44*, 687-705.
Ross, B.B. and Orlanski, I. 1978. The circulation associated with a cold front. Part II: Moist case. *J. Atmos. Sci., 35*, 445-65.
Rotunno, R. 1983. On the linear theory of the land and sea breeze. *J. Atmos. Sci., 40*, 1999-2009.
Ryan, B.F. and Wilson, K.J. 1985. The Australian summertime cool change. III: Subsynoptic and mesoscale model. *Mon. Weath. Rev., 113*, 224-40.
Sawyer, J.S. 1956. The vertical circulation at meteorological fronts and its relation to frontogenesis. *Proc. Roy. Soc., London, A234*, 346-62.
Smith, R.K. and Reeder, M.J. 1986. On the movement and low-level structure of cold fronts. *Monash University GFD Lab. Rep. No. 78*. Clayton, Australia.
Smith, R.K., Ryan, B.F., Troup, A.J. and Wilson, K.J. 1982. Cold fronts research: The Australian summertime 'cool change'. *Bull. Am. met. Soc., 63*, 1028-34.
Stone, P.H. 1966. Frontogenesis by horizontal wind deformation fields. *J. Atmos. Sci., 23*, 455-65.
Sun, W.-Y. and Ogura, Y. 1979. Boundary layer forcing as a possible trigger to squall-line formation. *J. Atmos. Sci., 36*, 235-54.
Thorpe, A.J. and Nash, C.A. 1984. Convective and boundary layer parameterisations in a diagnostic model of atmospheric fronts. *Q. Jl R. met. Soc., 110*, 443-66.
Thorpe, A.J. and Emanuel, K.A. 1985. Frontogenesis in the presence of small stability to slantwise convection. *J. Atmos. Sci., 42*, 1809-24.
Williams, R.T., Chou, L.C. and Cornelius, C.J. 1981. Effects of condensation and surface motion on the surface of steady-state fronts. *J. Atmos. Sci., 38*, 2365-76.
Williams, R.T. and Plotkin, J. 1968. Quasi-geostrophic frontogenesis. *J. Atmos. Sci., 25*, 201-6.
Wilson, K.J. and Stern, H. 1985. The Australian summertime and cool change. I: Synoptic and subsynoptic scale aspects. *Mon. Weath. Rev., 113*, 177-201.

Appendix

A parameterisation of dry buoyant convection

The first law of thermodynamics may be expressed as

$$\frac{d\Theta}{dt} = \frac{Q}{c_p\pi_e}. \qquad \text{...A.1}$$

Suppose that the only heat source is a sensible heat flux, $\dot{H}$, through the lower boundary and that the heat is uniformly and instantaneously distributed through a column of height h by turbulent mixing. Then, the specific rate of heating may be re-expressed as

$$\dot{Q} = \frac{\dot{H}}{\int_0^h \rho_o(z)dz}. \qquad \text{...A.2}$$

Combining Eqns A.1 and A.2 gives

$$\frac{d\Theta}{dt} = \frac{\dot{H}}{c_p\pi_e \int_0^h \rho_o(z)dz} \qquad \text{...A.3}$$

Assume that the sensible heat flux takes the form

$$\dot{H} = \begin{cases} A_o S_o \sin[\pi(t - t_s)/12] & t \geq t_s, x \geq 0 \\ 0 & \text{elsewhere,} \end{cases}$$

where $S_0 = 1380$ W m^{-2} is the solar constant and t_s is the time in hours when the heating begins. The adjustable constant, A_0, is taken to be 0.1 at $x = 0$ and 0.2 for $x > 0$. If convective mixing between the surface and higher levels were ignored, then, depending on the initial lapse rate, unstable vertical potential temperature gradients would eventually develop. The height of the mixed layer is assumed to be the minimum height required to redistribute the added heat without leaving the atmosphere unstable to convective overturnings. In this parameterisation, heat is mixed, but not momentum; thus, the convective Prandtl number is zero.

This scheme is implemented in the numerical model as follows:

$$h = m\Delta z$$

where m is the largest integer satisfying

$$\Theta(x,h - \Delta z/2,t) + \Delta\theta < \Theta(x,h + \Delta z/2,t)$$

and from Eqn A.3,

$$\Delta\theta \simeq \frac{\dot{H}\Delta t}{c_p\Delta z \sum_{i=1}^{m} \rho_o(i\Delta z)}$$